The crystal structure of mouse VDAC1 at 2.3 Å resolution reveals mechanistic insights into metabolite gating

Rachna Ujwal[a,b], Duilio Cascio[c], Jacques-Philippe Colletier[c], Salem Faham[a], Jun Zhang[a,b], Ligia Toro[d], Peipei Ping[a,b], and Jeff Abramson[a,1]

[a]Department of Physiology, [b]Cardiovascular Research Laboratories, [d]Department of Anesthesiology, Division of Molecular Medicine, David Geffen School of Medicine, and [c]Department of Energy Institute of Genomics and Proteomics, University of California, Los Angeles, CA 90095

Communicated by H. Ronald Kaback, University of California, Los Angeles, CA, September 29, 2008 (received for review September 3, 2008)

The voltage-dependent anion channel (VDAC) constitutes the major pathway for the entry and exit of metabolites across the outer membrane of the mitochondria and can serve as a scaffold for molecules that modulate the organelle. We report the crystal structure of a β-barrel eukaryotic membrane protein, the murine VDAC1 (mVDAC1) at 2.3 Å resolution, revealing a high-resolution image of its architecture formed by 19 β-strands. Unlike the recent NMR structure of human VDAC1, the position of the voltage-sensing N-terminal segment is clearly resolved. The α-helix of the N-terminal segment is oriented against the interior wall, causing a partial narrowing at the center of the pore. This segment is ideally positioned to regulate the conductance of ions and metabolites passing through the VDAC pore.

β-barrel | mitochondria | outer membrane protein | ATP flux

All eukaryotic cells require efficient exchange of metabolites between the cytoplasm and the mitochondria. This exchange is mediated by the most abundant protein in the outer mitochondrial membrane, the voltage-dependent anion channel (VDAC), which facilitates movement of ions and metabolites between the cytoplasm and the intermembrane space of the mitochondria. VDAC was first discovered in 1976 (1) and has since been extensively studied by a number of biochemical and biophysical techniques demonstrating its conserved properties of voltage gating and ion selectivity and its ability to act as a scaffold for modulator proteins from both sides of the outer membrane (2, 3).

Single-channel conductance experiments on VDAC1 at low membrane potential (10 mV) show a high conductance indicative of a large pore, often referred to as the open state of the channel (2). As voltage is increased (>30 mV) in either a positive or negative direction, a lower conductance, ostensibly the closed state, is obtained. Endogenous potentials caused by chemical gradients across the outer membrane [Donnan potentials (4)] may thus be sufficient to regulate this channel. Although the nature of either of these states is unknown in the absence of structural data, transition between them presumably involves conformational changes constituting a gating action that hinders the passage of metabolites such as adenine nucleotides. Furthermore, this transition is associated with altered ion selectivity because the channel shifts from weakly anion selective to weakly cation selective as it moves from open to closed. This complex gating behavior has driven numerous investigations that have provided sometimes contradictory findings; however, the role of VDAC to regulate metabolite traffic across the outer membrane is firmly established.

As the major pathway into and out of mitochondria, VDAC mediates an intimate dichotomy between metabolism and death in all cells (5). Mitochondrial-dependent cell death involves numerous proteins [including hexokinase (6) and the Bcl-2 family of proteins (7), in particular] that alternatively promote or prevent mitochondrial dysfunction through interaction with, and potentially modification of, VDAC. Alterations in mitochondrial permeability have been implicated in the metabolic stresses of cancer (8) and cardiovascular disease (9). Therefore, the ability to modulate VDAC function in a rational manner will have important implications for novel therapeutics to modulate cell survival in different diseases (10). We have determined the structure of the murine VDAC1 (mVDAC1) at 2.3 Å resolution crystallized in a lipidic environment. In addition to providing concise structural details that can aid drug design, the high-resolution structure of mVDAC1 reveals insights into the gating mechanism for metabolites and ions entering and exiting mitochondria.

Results

We have expressed and purified mVDAC1 based on a procedure by Koppel *et al.* (11) with extensive modifications. After purification, the protein was shown to be folded by circular dichroism (data not shown). mVDAC1 was functionally characterized in planar lipid bilayers where it exhibited single-channel conductance of 3.7 ± 0.4 nS at 10 mV in 1 M KCl [open state; supporting information (SI) Fig. S1]. As the applied voltage was increased to ± 30 mV, the channel shifted to a predominant conductance of 1.7 ± 0.2 nS (closed state; Fig. S1). These values are in good agreement with those recorded for endogenous VDAC1 isolated from rat (12). To understand functional aspects of ion and metabolite trafficking and the complex gating pattern observed electrophysiologically, we pursued the task of obtaining a high-resolution structure of mVDAC1.

Circular dichroism (CD) studies have shown that human VDAC1 (hVDAC1) exhibits different contents of secondary structure in detergent micelles as compared with phospholipid bilayers, with the latter displaying a higher content of β-sheet and a lower content of α-helix (13). Because a majority of the functional studies have been performed in phospholipid bilayers (2, 14) and it is assumed that under lipidic conditions VDAC would more closely resemble a "native" conformation, we crystallized mVDAC1 in 1,2-Dimyristoyl-sn-Glycero-3-Phosphocholine (DMPC)/3-[(3-cholamidopropyl)dimethylammonio]-2-hydroxy-1-propanesulfonate (CHAPSO) bicelles (15) using 2-methyl-2,4-pentanediol (MPD) as a precipitant. In contrast to crystallization in detergent micelles, bicelles are small bilayer-

Author contributions: P.P. and J.A. designed research; R.U. and J.Z. performed research; D.C., J.-P.C., and S.F. contributed new reagents/analytic tools; R.U., D.C., J.-P.C., L.T., and J.A. analyzed data; and J.A. wrote the paper.

The authors declare no conflict of interest.

Data deposition: The atomic coordinates have been deposited in the Protein Data Bank, www.pdb.org (PDB ID code 3EMN).

[1]To whom correspondence should be addressed. E-mail: jabramson@mednet.ucla.edu.

This article contains supporting information online at www.pnas.org/cgi/content/full/0809634105/DCSupplemental.

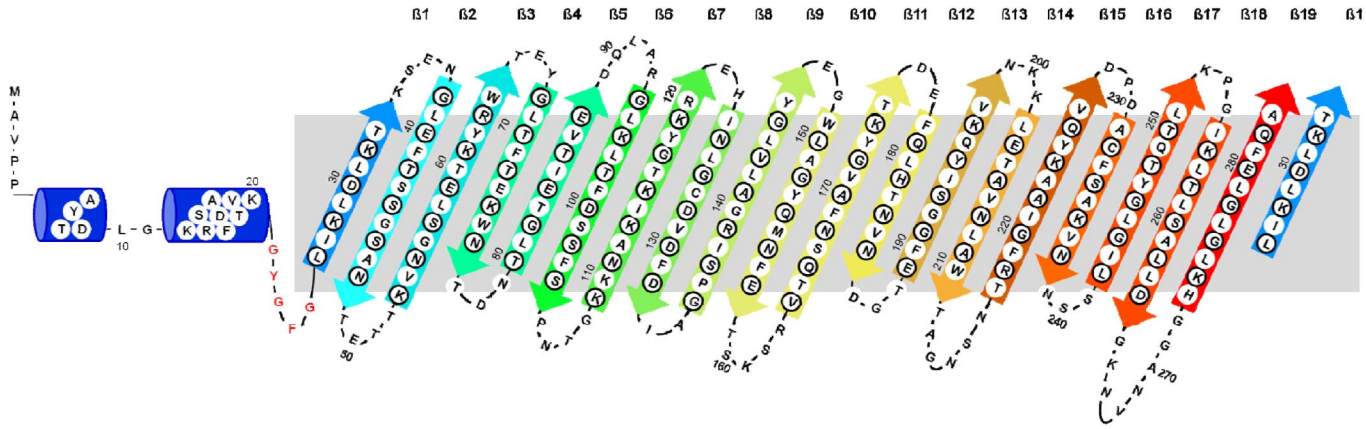

Fig. 1. Secondary structure schematic of mVDAC1. The mVDAC1 protein structure is colored from the N terminus in blue to the C terminus in red. The β-strands and α-helix are depicted as arrows and cylinders, respectively, and are colored by using single-letter amino acid code. β-Strand residues facing the inside of the pore are shown with a black border. Residues in red form the hinge region.

like discs that more closely mimic the native lipid environment. As a result, the structure we present here likely represents that of the endogenous channel.

Structural Overview. Optimized crystals of mVDAC1 belong to the monoclinic space group C2 with 1 molecule per asymmetric unit. The structure was solved by the single isomorphous replacement with anomalous scattering (SIRAS) technique by using an engineered cysteine to incorporate a single mercury atom, a method that was successfully used for LacY (16) and vSGLT (17). The model was refined from merged data to a resolution of 2.3 Å with R_{free} of 27.7% and R_{work} of 24.2% (Table S1). All 283 amino acids of mVDAC1 were built along with 47 water molecules. Thus, all structural features represented in this study, including the location of the N-terminal segment, were assigned on the basis of high-resolution data. Further details regarding the crystallization and structure determination can be found in *Methods*. Experimental and refined electron density maps are shown in Fig. S2.

Predictions regarding the number of strands contained in the VDAC β-barrel varied widely with 2 values in particular, 13 (18) and 16 (19, 20), emerging as the predicted number of β-strands. The structure of the mVDAC1 protomer forms a β-barrel composed of 19 β-strands with a shear number of 23 (Figs. 1 and 2). All of the strands exhibit an antiparallel pattern with the exception of strands 1 and 19 that associate in a parallel manner to close the barrel (Fig. 2*A*). The maximal height and width of the β-barrel is 35 and 40 Å, respectively. This report illustrates the high-resolution crystal structure of a eukaryotic β-barrel membrane protein with an odd number of strands (all known

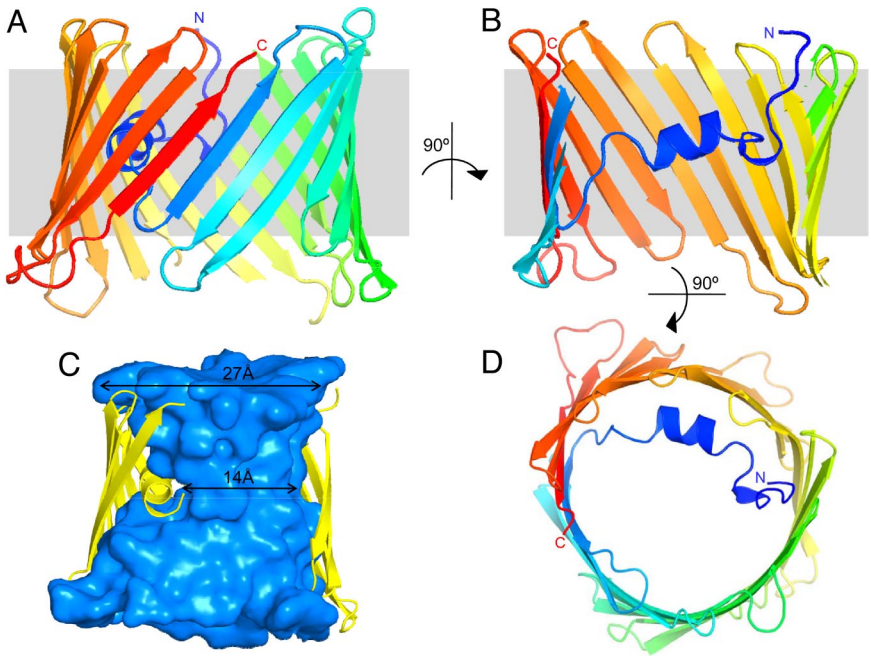

Fig. 2. Overall structure of mVDAC1. (*A*) Cartoon representation of mVDAC1 viewed parallel to the plane of the membrane. The mVDAC1 protein structure is colored from the N terminus in blue to the C terminus in red. (*B*) Cross-section view of *A* rotated 90° clockwise. β-Strands 3–7 are removed to illustrate positioning of the N-terminal segment. (*C*) Cross-section view of *A* with β-strands 19 and 1–4 removed. The interior surface of the mVDAC1 channel (cyan), created using the program HOLLOW (http://hollow.sourceforge.net), illustrates the contour of the pore. Dimensions at the entrance and along the narrowest point in the center of the pore are displayed. (*D*) Cartoon representation of mVDAC1 viewed perpendicular to the membrane plane (same coloring as in *A*).

prokaryotic β-barrels have an even number of strands), confirming the architecture observed in the recent NMR study on hVDAC1 (21).

The correct orientation of the protein within the outer membrane of the mitochondria cannot be ascertained from the structure presented herein, because there have been multiple biochemical studies producing conflicting results on the endogenous position of the N and C termini (22–24) (i.e., whether they are facing the cytosol or intermembrane space). The hydrophilic N terminus of the protein forms a distorted α-helix that is nestled within the pore and tethered to the first β-strand. Both the N and C termini reside on the same side of the membrane and clearly demonstrate that the N terminus is not embedded in the membrane as has been suggested (18).

The orifice of the pore resembles a slightly elliptical cylinder with a maximal inner dimension of 27 × 24 Å (Fig. 2*C*). The pore forms a large pathway that transcends the entire length of the protein, likely representing the open conformation of the channel. These dimensions are in good agreement with those reported by electron microcopy (25), atomic force microscopy (26), and the recently published NMR structure of hVDAC1 (21). Structural alignments between the crystal structure of mVDAC1 and the 20 deposited NMR structures of hVDAC1 (Protein Data Bank ID code 2K4T) showed an rmsd that varied from 1.72 to 4.68 Å (the average rmsd among all 20 NMR structures is 4.79 Å) (Fig. S3). In the NMR study, only 5 residues were assigned in the voltage-sensing N-terminal segment (residues 6–10). These studies were performed on hVDAC1 solubilized in detergent micelles, which may be responsible for the high degree of mobility. The structure presented here at 2.3 Å is that of mVDAC1 crystallized in lipidic bicelles. This high-resolution image reveals structural insights into the conduction pathway and moreover the precise localization and structural features of the voltage-sensing N-terminal segment. The assignment of the N-terminal segment is essential, because this helix plays a crucial role in gating the pore.

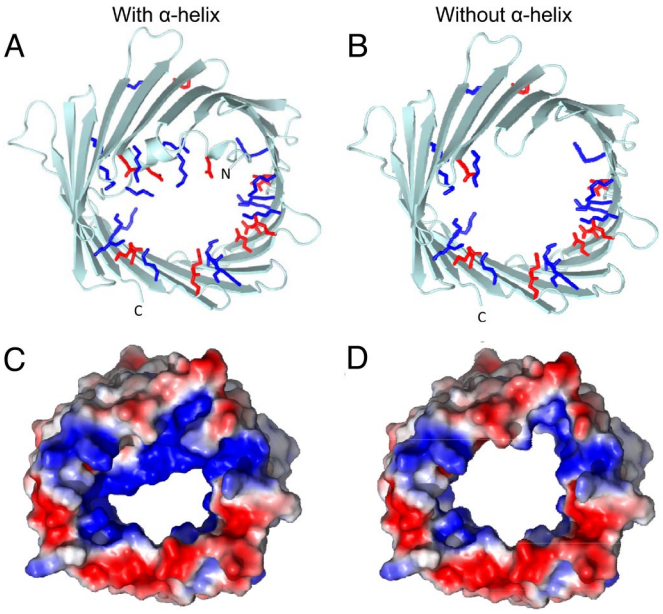

Fig. 3. Charge distribution and electrostatic potential of the mVDAC1 pore. (*A*) Cartoon representation of mVDAC1 (viewed perpendicular to the membrane plane) showing symmetrical charge distribution along β-strands 1–8 and the N-terminal α-helix. Residues with positive (Arg and Lys) and negative (Glu and Asp) charges are colored blue and red, respectively. (*B*) Same as in *A* without the α-helix, depicting the reduced number of charged residues on β-strands 9–19 (located behind the α-helix). (*C* and *D*) Electrostatic potential, calculated by using the nonlinear Poisson–Boltzmann equation, is displayed on the surface-accessible surface at a contour level of ± 2 KT. Positive and negative charges are colored blue and red, respectively. mVDAC1 is viewed perpendicular to the membrane plane with the helix present (*C*) or absent (*D*). Note that the presence of the N-terminal segment (*A* and *C*) engenders a high positive charge density, whereas in its absence the wall of the β-barrel harbors a reduced charge density (*B* and *D*).

Characteristics of the Pore. The exterior of the β-barrel primarily consists of hydrophobic residues that are exposed to the lipid environment, whereas the interior is extensively hydrophilic, which is conducive for the efficient passage of ions and large metabolites (Fig. 3). Analysis of the interior walls of the pore reveals 15 positively-charged residues and 11 negatively-charged residues (Fig. 3). These charged residues are not uniformly distributed along the β-strands of the barrel, but are clustered primarily along strands 1–8. In contrast, there are fewer charged residues present on β-strands 9–19 (Fig. 3 *B* and *D*). The pore spanning N-terminal α-helical segment contains 3 positive (Lys-12, Lys-20, and Arg-15) and 2 negative (Asp-9 and Asp-16) charges facing the interior of the pore. Electrostatic calculations (Fig. 3 *C* and *D*) show that the interior of the pore has a higher density of positive versus negative charges, a fact that could account for the channel's preference for transporting anions over cations in the open conformation (2). The α-helix of the N-terminal segment is located approximately halfway down the pore, resulting in a partial narrowing of the cavity to 27 × 14 Å (Fig. 2*C*), yet there is still ample space for the passage of metabolites. Thus the structure presented here likely represents the open conformation. This charged α-helix is ideally positioned to regulate the conductance of ions and metabolites passing through the VDAC pore.

Arrangement and Coordination of the N-Terminal Helix. Numerous studies have focused on the importance of the N-terminal α-helical segment's role in channel function. There has been a wide range of predictions as to the functional disposition of this domain, ranging from forming a segment of the channel wall (22, 27) to acting as the voltage sensor (2, 11). In 2007, De Pinto *et al.* (28) used NMR to resolve a peptide fragment of the N terminus (Prn2–20) corresponding to amino acids 2–20 of hVDAC1. Their findings show a complex behavior of the N-terminal domain where the peptide is unstructured in aqueous solvent and forms a well-ordered α-helix from residues 5–16 in SDS. In the recently reported NMR structure of hVDAC1, an accurate analysis of the structure of the N-terminal segment and its localization with respect to the rest of the protein was not possible because of the incomplete assignment of this region (residues 1–5 and 11–20 unassigned) (21).

However, our high-resolution structure presented herein shows the N-terminal segment (amino acids 1–26) forming a hydrogen-bonding pattern that facilitates its orientation against the interior wall of the pore (Fig. 4*A*) adjacent to β-strands 8–19. The first 5 N-terminal amino acids extend down the pore where 2 hydrogen bonds are observed between the carbonyl oxygens of Ala-2 and Pro-4 and the main-chain nitrogen of His-122 and ND2 of Asn-124, which are located on the wall of the pore. These interactions stabilize the N terminus to β-strand 8. Continuing in a C-terminal direction down the protein, a distorted helix is formed from amino acids 6–20 where the hydrogen-bonding pattern is broken at Leu-10 and Gly-11, separating the helix into 2 segments. Although the stable helical hydrogen-bonding pattern is disrupted, these 2 segments are capable of maintaining a rigid structure because Arg-15 forms bridging bidentate hydrogen bonds with the carbonyl oxygens from Ala-8 and Leu-10 (Fig. 4*B*). The helical portion of the N-terminal segment has 2 hydrogen bonds to β-strands 12 and 16, stabilizing its interaction with the wall of the pore. Connecting the soluble N-terminal domain to the first β-strand of the barrel is a highly conserved

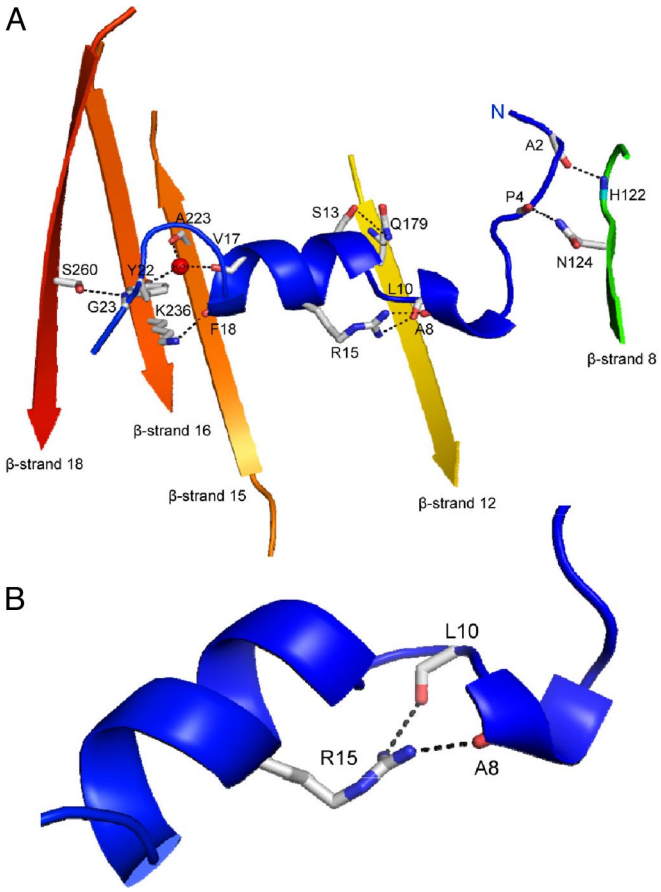

Fig. 4. The soluble N-terminal segment of mVDAC1. (*A*) The hydrogen-bonding pattern of the N-terminal segment facilitates its orientation against the interior wall of the pore. Only residues involved in bonding between the β-barrel wall and the soluble N-terminal domain are indicated. (*B*) Blow-up view of the N-terminal α-helix showing bridging bidentate hydrogen bond between Arg-15 and the carbonyl oxygens of Ala-8 and Leu-10.

sequence (among mammals) of Gly-21–Tyr-22–Gly-23–Phe-24–Gly-25 (Fig. 1). This portion of the N-terminal segment is hydrogen-bonded to β-strands 16 and 18.

Discussion

We present here the high-resolution crystal structure of a eukaryotic outer mitochondrial membrane protein. Our findings report a detailed high-resolution structure of a class of β-barrel membrane proteins formed by a 19-stranded β-sheet. The odd number of strands, which has not been observed in any of the previous β-barrel structures, requires strands 1 and 19 to associate in a parallel configuration (all other strands arrange in an antiparallel manner), which results in weaker hydrogen bonding along this interface. Although now synthesized from the nuclear genome, VDAC has the interesting distinction of being a likely holdover from when mitochondria were symbiotic bacteria during the evolution of early eukaryotes (29). It is intriguing to speculate as to whether the difference in strand number and the mechanistic importance of the N-terminal broken helix in mVDAC1 as compared with bacterial porins are clues into the functional evolution of this protein from its prokaryotic origin to the eukaryotic form.

Physiological Modulators of VDAC. As predicted, VDAC has a large hydrophilic pore capable of facilitating the passage of ions and large metabolites such as ATP. There have been a number of reports suggesting the channel may have specific nucleotide binding sites (2, 30). To address this issue, we attempted to identify an ATP binding site in the structure of mVDAC1. We resolved the structures of mVDAC1 in the presence of 5, 10, 50, and 100 mM ATP, but the corresponding structures revealed no additional electron density that would correspond to ATP. Similarly, we have crystallized mVDAC1 in the presence of other known nucleotide modulators (ADP and AMP-PNP) and observed no changes in the mVDAC1 structure, as determined by inspection of $F_{o(\text{nucleotide})} - F_{o(\text{native})}$ maps. We therefore conclude that, at least in this conformation, there is likely no stable or specific binding site for these nucleotides.

Previous studies have shown that Ca^{2+} binds and regulates VDAC (31, 32), a result with clear implications for the role of the protein in mitochondrial-dependent cell death. Under initial crystallization conditions (where trace Ca^{2+} may be present), we were unable to identify electron density or a coordination pattern that resembles Ca^{2+} ligation. To further address this issue we solved the structure of mVDAC1 in the presence of 25 mM EGTA (a calcium-chelating agent that should bind all Ca^{2+} ions in solution and from the protein) and separately in the presence of 25 mM $CaCl_2$. Crystals formed in the presence of EGTA, and separate successful crystallization trials in the presence of $AlCl_3$ or $InCl_3$ were indistinguishable from the initial conditions with trace Ca^{2+}. When Ca^{2+} is present in abundance, we observe electron density near Glu-73 that is indicative of metal ion coordination between 2 antiparallel mVDAC1 monomers (Fig. S4). De Pinto *et al.* (33) had shown that Glu-73 is buried in a hydrophobic environment, an observation that is explained by the current structure, which demonstrates its localization within the membrane. Furthermore, mutagenesis and functional analyses have implicated this residue in Ca^{2+} binding (32) and hexokinase-mediated protection against mitochondrial-dependent cell death (34). Based on the data presented here, Ca^{2+} must be present at excessive concentrations for stable binding to the protein. The only way this could happen endogenously would be with enormous levels of Ca^{2+} present and/or other gross disruption of the lipid interface with the outside of the pore, events that may occur during mitochondrial-dependent cell death.

Interestingly, crystallization in the presence of Mg^{2+}–ATP results in a very similar localization pattern of the Mg^{2+} as was observed for Ca^{2+} at position Glu-73 of the crystal antiparallel dimer (Fig. S4). As was the case in the presence of ATP alone, this crystallization scenario does not reveal stable or specific binding site for the nucleotide. As mentioned above, Glu-73 is essential for the binding of the antiapoptotic protein hexokinase to VDAC (34). It is well established that the hydrophobic N terminus of hexokinase is required for its interactions with mitochondria (35), presumably through insertion into the membrane. Furthermore, high concentrations of Mg^{2+} are required for hexokinase to associate with the mitochondria (36). Thus, Mg^{2+} coordination to Glu-73 may reveal a structural feature that facilitates association of the N-terminal segment of hexokinase with the external surface of the VDAC pore, a process likely to be concomitant with inhibition of mitochondrial-dependent cell death.

Regulation of VDAC Permeability. It is well established that VDAC is the principal governor for the exchange of metabolites between the intermembrane space of the mitochondria and the cytosol. The structure presented here reveals a number of features that are consistent with the open conformation of the channel and provides a possible mechanism for regulating the flow of metabolites. The arrangement of charges in the wall of the β-barrel are clustered primarily on the first half of the pore (strands 1–8), whereas the second half is less hydrophilic (β-strands 9–19). In this second half of the pore, the soluble N-terminal segment descends into the cavity forming a distorted

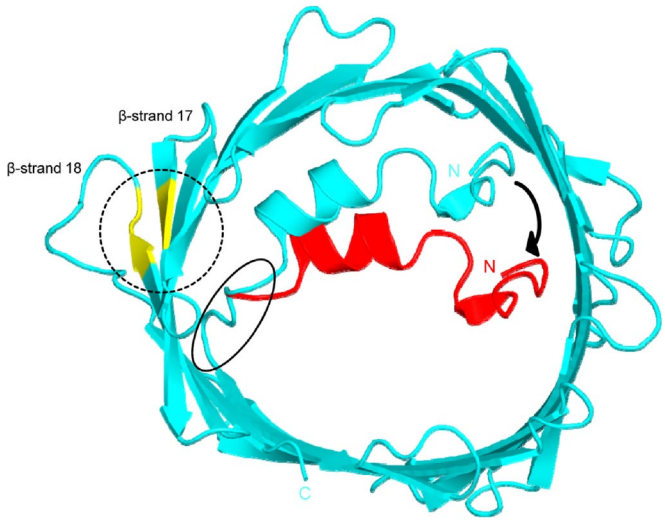

Fig. 5. Proposed model of the transition from open to closed state. The structure of mVDAC1 obtained from this study is colored cyan and displayed as viewed perpendicular to the membrane. The region predicted to interact with NADH (21) is colored yellow and indicated by a dashed circle. The solid circle surrounds the proposed hinge region (Gly-21–Tyr-22–Gly-23–Phe-24–Gly-25). The α-helix in red represents the proposed model of a closed state. The model was made by 10° rotation along the horizontal axis of the protein at the hinge region and would produce a conformation sufficient to perturb metabolite flux. As detailed in *Discussion*, the structure indicates that this hypothetical occluded state could be stabilized by interactions of the soluble N-terminal domain with the opposite wall of the pore.

α-helix (amino acids 6–20) containing 5 charged residues that face toward the aqueous environment. In this configuration the helix, rather than the β-barrel, contributes to a symmetrical charge distribution (Fig. 3).

There is a general consensus that the N-terminal segment of VDAC is involved in voltage gating and therefore it may adopt different conformations depending on factors external to the protein (e.g., protein–protein interactions, ion interactions, lipid environment). In our crystals, the α-helix portion of the N-terminal segment is positioned halfway down the pore, causing a narrowing of the cavity (27 × 14 Å) (Fig. 2*C*). This constriction site is ideally situated to regulate the flow of metabolites. The connection from the α-helix to the first β-strand is a flexible and highly conserved sequence (Gly-21–Tyr-22–Gly-23–Phe-24–Gly-25). The alternating glycine residues are well suited to perform a hinge function, facilitating rearrangement of the helix in response to stimuli. Specifically, rotation at this hinge region to move the helix away from the wall of the pore would place the N-terminal domain into a position of greater obstruction within the cavity where it would block the transport of metabolites while still permitting ion flux (Fig. 5).

What Are the Structural Rearrangements Underlying Such a Movement of the N-Terminal Gating Helix? There are a number of stimuli known to favor the closed state of the channel: voltage potentials in excess of ± 30 mV (37), protein interactions (38), and chemical modulators like NADH (2). These stimuli may disrupt the hydrogen bonds that position the N-terminal segment along the interior wall of the β-barrel. Once interactions with the wall of the pore are disrupted, the N-terminal segment would be free to reorient within the channel lumen aided by the flexibility in the hinge region. At this point, the repositioning of the α-helix may be facilitated by the protein's inherent chemical potential: electrostatic calculations reveal a cluster of positive charges along the α-helix and a patch of negative charges located on the opposing wall (β-strands 2, 3, 5, 6, and 8) in the region where the helix could possibly interact if VDAC were to adopt the more occlusive conformation of the pore. Mutational data from the Colombini group (39) support this hypothesis, wherein substitutions of residues forming the N-terminal α-helix alter voltage-dependent gating in a charge-dependent manner. Alternatively, the 2 segments of the α-helix portion are joined by bridging bidentate hydrogen bonds from Arg-15 (Fig. 4*B*). Perturbation of this interaction could also impair metabolite flux by repositioning of amino acids 1–10.

Further evidence in support of alterations in the position of the α-helix came from the recent NMR structure of hVDAC1. Hiller and colleagues (21) report an NADH interaction site on β-strands 17 and 18 involving residues at position Leu-242, Ile-243, Gly-244, Ala-261, Leu-263, and Asp-264 (residues from hVDAC1) (Fig. 5). NADH has been shown to favor the closed state of the channel (2), and the interaction site described above flanks the hinge region of the N-terminal segment as determined from the data in the present study. Our structure clearly demonstrates that there is insufficient space for NADH binding in this region. Hence, the N-terminal segment would have to be repositioned to accommodate NADH and in doing so would close the channel.

As is the case with most high-resolution structures, many critical features of the protein's anatomy have been identified, explaining several key features of its physiological behavior. However, many new questions also arise that will require additional structure and functional studies to answer. The structure and hypothesized mechanism of mVDAC1 presented herein establish a template to be tested by biochemical/biophysical techniques and provides critical information for our understanding of mitochondrial biology.

Methods

Expression, Purification, and Refolding. The expression and purification protocol was adapted from Koppel *et al.* (11) with extensive modifications. Briefly, histidine-tagged mVDAC1 was expressed in *Escherichia coli* and the inclusion bodies (IB) were isolated. Solubilized IB were purified by using a Talon affinity column and refolded by using n-dodecyl-N,N-dimethylamine-N-oxide. Refolded protein was applied to a Superdex 75 column for isolation of a homogenous protein population. More details can be found in *SI Text*.

Single-Channel Conductance Measurements. The single-channel conductance across black lipid bilayers was recorded as described (13). More details can be found in the *SI Text*.

Crystallization and Structure Determination. Bicelles were prepared as described (15). Purified mVDAC1 at a concentration of 15 mg/ml was mixed in a 4:1 protein/bicelle ratio with a 35% (2.8:1) DMPC/CHAPSO bicellar solution, giving 12 mg/ml mVDAC1 in 7% bicelles. Our best crystals grew at 20°C in 18–20% MPD, 0.1 M Tris·HCl (pH 8.5) with 10% PEG400 added to the protein drop only. Heavy atom labeling of single cysteine constructs was done by using methyl mercuric acetate. Native data were collected at the Advanced Light Source (Berkeley, CA) at beamline 5.0.2, and Hg-derivative data were collected at the Advanced Photon Source (Chicago) at the microfocal beamline 24-ID-E. Both native and derivative data were processed by using the program DENZO (40).

One heavy atom site was found for Cys-127, and SIRAS phases were calculated in PHENIX and MLPHARE (41). Density modification was done by using DM from the CCP4 package (42). Diffraction data from 20–2.3 Å were used for refinement and electron-density map calculations. Graphic operations and model building were performed with COOT (43). Refinement and map calculations were performed by using PHENIX version 1.3 (44) and CNS version 1.2 (45). At the end of the refinement, the $F_o - F_c$ map was virtually featureless at ± 3 sigma. Figures were produced with PyMOL (www.pymol.org). Molecular topologies and parameters of DMPC were created by using ELBOW in PHENIX. The quality of the structure was checked and validated by using PROCHECK. Refinement statistics are shown in Table S1.

ACKNOWLEDGMENTS. We thank R. Kaback, T. Vondriska, M. Sawaya, M. Grabe, G. Wagner, and K. Zeth for critical discussion; T. Vondriska for comments on the manuscript; D. Eisenberg for generous use of resources; V.

Chaptal and A. Laganowsky for assistance with data collection; P. Souda and J. Whitelegge for assistance with the ESI-MS and tandem mass spectroscopy; University of California–Los Angeles Physiology Protein Expression Core for protein production; University of California–Los Angeles Department of Energy X-Ray Crystallography Core Facility for assistance with structure determination; and The Advance Light Source (P. Zwart and beamline staff at 5.0.2) and the Advance Photon Source (M. Capel, K. Rajashankar, J. Schuermann, and I. Kourinov at NECAT 24-ID-E) for data collection and assistance in structure determination. This work was supported by National Institutes of Health Grants PO1-080111 (to P.P.), HL-080691 (to P.P.), HL-68901 (to P.P.), and GM07844 (to J.A.); Human Frontier Science Program Grant RGY0069 (to J.A.); and American Heart Association Grant 0630258N (to J.A.).

1. Schein SJ, Colombini M, Finkelstein A (1976) Reconstitution in planar lipid bilayers of a voltage-dependent anion-selective channel obtained from paramecium mitochondria. *J Membr Biol* 30:99–120.
2. Colombini M, Blachly-Dyson E, Forte M (1996) VDAC, a channel in the outer mitochondrial membrane. *Ion Channels* 4:169–202.
3. Rostovtseva TK, Bezrukov SM (2008) VDAC regulation: Role of cytosolic proteins and mitochondrial lipids. *J Bionenerg Biomembr* 40:163–170.
4. Porcelli AM, *et al.* (2005) pH difference across the outer mitochondrial membrane measured with a green fluorescent protein mutant. *Biochem Biophys Res Commun* 326:799–804.
5. Lemasters JJ, Holmuhamedov E (2006) Voltage-dependent anion channel (VDAC) as mitochondrial governator: Thinking outside the box. *Biochim Biophys Acta* 1762:181–190.
6. Nakashima RA, Mangan PS, Colombini M, Pedersen PL (1986) Hexokinase receptor complex in hepatoma mitochondria: Evidence from *N,N′*-dicyclohexylcarbodiimide-labeling studies for the involvement of the pore-forming protein VDAC. *Biochemistry* 25:1015–1021.
7. Shimizu S, Narita M, Tsujimoto Y (1999) Bcl-2 family proteins regulate the release of apoptogenic cytochrome *c* by the mitochondrial channel VDAC. *Nature* 399:483–487.
8. Galluzzi L, Kepp O, Tajeddine N, Kroemer G (2008) Disruption of the hexokinase-VDAC complex for tumor therapy. *Oncogene* 27:4633–4635.
9. Weiss JN, Korge P, Honda HM, Ping P (2003) Role of the mitochondrial permeability transition in myocardial disease. *Circ Res* 93:292–301.
10. Simamura E, Shimada H, Hatta T, Hirai KI (2008) Mitochondrial voltage-dependent anion channels (VDACs) as novel pharmacological targets for anticancer agents. *J Bionenerg Biomembr* 40:213–217.
11. Koppel DA, *et al.* (1998) Bacterial expression and characterization of the mitochondrial outer membrane channel. Effects of n-terminal modifications. *J Biol Chem* 273:13794–13800.
12. Colombini M (1989) Voltage gating in the mitochondrial channel, VDAC. *J Membr Biol* 111:103–111.
13. Shanmugavadivu B, *et al.* (2007) Correct folding of the β-barrel of the human membrane protein VDAC requires a lipid bilayer. *J Mol Biol* 368:66–78.
14. Rostovtseva TK, Tan W, Colombini M (2005) On the role of VDAC in apoptosis: Fact and fiction. *J Bionenerg Biomembr* 37:129–142.
15. Faham S, Bowie JU (2002) Bicelle crystallization: A new method for crystallizing membrane proteins yields a monomeric bacteriorhodopsin structure. *J Mol Biol* 316:1–6.
16. Abramson J, *et al.* (2003) Structure and mechanism of the lactose permease of *Escherichia coli*. *Science* 301:610–615.
17. Faham S, *et al*. (2008) The crystal structure of a sodium galactose transporter reveals mechanistic insights into Na^+/sugar symport. *Science* 321:810–814.
18. Song J, *et al.* (1998) The topology of VDAC as probed by biotin modification. *J Biol Chem* 273:24406–24413.
19. Casadio R, Jacoboni I, Messina A, De Pinto V (2002) A 3D model of the voltage-dependent anion channel (VDAC). *FEBS Lett* 520:1–7.
20. Young MJ, Bay DC, Hausner G, Court DA (2007) The evolutionary history of mitochondrial porins. *BMC Evol Biol* 7:31.
21. Hiller S, *et al.* (2008) Solution structure of the integral human membrane protein VDAC-1 in detergent micelles. *Science* 321:1206–1210.
22. De Pinto V, *et al.* (1991) Peptide-specific antibodies and proteases as probes of the transmembrane topology of the bovine heart mitochondrial porin. *Biochemistry* 30:10191–10200.
23. Engelhardt H, *et al.* (2007) High-level expression, refolding, and probing the natural fold of the human voltage-dependent anion channel isoforms I and II. *J Membr Biol* 216:93–105.
24. Stanley S, Dias JA, D'Arcangelis D, Mannella CA (1995) Peptide-specific antibodies as probes of the topography of the voltage-gated channel in the mitochondrial outer membrane of *Neurospora crassa*. *J Biol Chem* 270:16694–16700.
25. Mannella CA (1982) Structure of the outer mitochondrial membrane: Ordered arrays of porelike subunits in outer-membrane fractions from *Neurospora crassa* mitochondria. *J Cell Biol* 94:680–687.
26. Goncalves RP, *et al.* (2007) Supramolecular assembly of VDAC in native mitochondrial outer membranes. *J Mol Biol* 369:413–418.
27. Forte M, Guy HR, Mannella CA (1987) Molecular genetics of the VDAC ion channel: Structural model and sequence analysis. *J Bionenerg Biomembr* 19:341–350.
28. De Pinto V, *et al*. (2007) Determination of the conformation of the human VDAC1 N-terminal peptide, a protein moiety essential for the functional properties of the pore *Chembiochem* 8:744–756.
29. Wallace DC (2005) A mitochondrial paradigm of metabolic and degenerative diseases, aging, and cancer: A dawn for evolutionary medicine *Annu Rev Genet* 39:359–407.
30. Yehezkel G, *et al.* (2006) Nucleotide-binding sites in the voltage-dependent anion channel: Characterization and localization. *J Biol Chem* 281:5938–5946.
31. Bathori G, *et al.* (2006) Ca^{2+}-dependent control of the permeability properties of the mitochondrial outer membrane and voltage-dependent anion-selective channel (VDAC). *J Biol Chem* 281:17347–17358.
32. Israelson A, *et al.* (2007) Localization of the voltage-dependent anion channel-1 Ca^{2+}-binding sites. *Cell Calcium* 41:235–244.
33. De Pinto V, al Jamal JA, Palmieri F (1993) Location of the dicyclohexylcarbodiimide-reactive glutamate residue in the bovine heart mitochondrial porin. *J Biol Chem* 268:12977–12982.
34. Zaid H, *et al.* (2005) The voltage-dependent anion channel-1 modulates apoptotic cell death. *Cell Death Differ* 12:751–760.
35. Xie GC, Wilson JE (1988) Rat brain hexokinase: The hydrophobic N terminus of the mitochondrially bound enzyme is inserted in the lipid bilayer. *Arch Biochem Biophys* 267:803–810.
36. Felgner PL, Wilson JE (1977) Effect of neutral salts on the interaction of rat brain hexokinase with the outer mitochondrial membrane. *Arch Biochem Biophys* 182:282–294.
37. Colombini M (1979) A candidate for the permeability pathway of the outer mitochondrial membrane. *Nature* 279:643–645.
38. Cheng EH, *et al.* (2003) VDAC2 inhibits BAK activation and mitochondrial apoptosis. *Science* 301:513–517.
39. Thomas L, Blachly-Dyson E, Colombini M, Forte M (1993) Mapping of residues forming the voltage sensor of the voltage-dependent anion-selective channel. *Proc Natl Acad Sci USA* 90:5446–54469.
40. Otwinowski Z, Minor W (1997) Processing of X-ray diffraction data collected in oscillation mode. *Methods Enzymol* 276:307–326.
41. Adams PD, *et al.* (2002) PHENIX: Building new software for automated crystallographic structure determination. *Acta Crystallogr D* 58:1948–1954.
42. Collaborative Computational Project (1994) The CCP4 suite: Programs for protein crystallography. *Acta Crystallogr D* 50:760–763.
43. Emsley P, Cowtan K (2004) Coot: Model-building tools for molecular graphics. *Acta Crystallogr D* 60:2126–2132.
44. Adams PD, *et al.* (2004) Recent developments in the PHENIX software for automated crystallographic structure determination. *J Synchrotron Radiat* 11:53–55.
45. Brunger AT, *et al.* (1998) Crystallography and NMR system: A new software suite for macromolecular structure determination. *Acta Crystallogr D* 54:905–921.